Available online at www.sciencedirect.com
SCIENCE DIRECT
Journal of Colloid and Interface Science 298 (2006) 615–623
JOURNAL OF Colloid and Interface Science
www.elsevier.com/locate/jcis

The impact of Mn oxide coatings on Zn distribution

Thipnakarin Boonfueng [a], Lisa Axe [a,*], Ying Xu [a], Trevor A. Tyson [b]

[a] *Department of Civil and Environmental Engineering, New Jersey Institute of Technology, University Heights, Newark, NJ 07102, USA*
[b] *Department of Physics, New Jersey Institute of Technology, University Heights, Newark, NJ 07102, USA*

Received 5 December 2005; accepted 12 January 2006

Available online 8 February 2006

Abstract

Zinc sorption to hydrous manganese oxide (HMO)-coated clay was investigated macroscopically, kinetically, and spectroscopically. Adsorption edges and isotherms revealed that the affinity and capacity of the HMO-coated montmorillonite was greater than that of montmorillonite, and when normalized to the oxide present, the coatings behaved similarly to the discrete Mn oxide. Over two pH conditions, 5 and 6, a linear relationship was observed for the isotherms; further analysis with X-ray absorption spectroscopy (XAS) resulted in one type of sorption configuration as a function of loading and ionic strength at pH 5. However, at a surface loading of 10^{-3} $\mathrm{mol_{Zn}\,g^{-1}_{HMO\text{-}coated\ clay}}$ when the pH increased from 5 to 7, the first shell distance decreased slightly, while the atoms and coordination numbers remained the same; this change may be attributed to an increase in electrostatic interactions. After a contact time of 4 months where an additional 60% of the sites become occupied, the slower sorption process was modeled as intraparticle surface diffusion. Best fit diffusivities ranged from 10^{-18} to 10^{-17} $\mathrm{cm^2/s}$, where a slower process was observed for the coated surface as compared to the discrete oxide. Interestingly, the porosity of the Mn oxide coating appears to be influenced by the substrate during its growth, as its increase and shift to a smaller pore size distribution resulted in a diffusivity between that observed for discrete HMO and montmorillonite.

Keywords: Zn; Sorption; XAS; Manganese oxide; Montmorillonite; HMO-coated montmorillonite; Intraparticle surface diffusion

1. Introduction

Oxides of manganese are important components in soils and sediments and major sinks for metals released into the environment from various sources [1–6]. Although a number of researchers [6–10] have studied manganese oxides, little is known about their interactions with clay. The association of oxide and clay minerals has been observed naturally as an integral part of soils, sediments, and stream deposits where Mn oxides form abiotically and biotically [11–15]. In an earlier study [16], we evaluated the surface properties and molecular structure of hydrous Mn oxide (HMO)- and crystalline Mn oxide-coated montmorillonite. These surface oxide coatings resulted in a larger surface area that dominated the surface charge, potentially controlling metal mobility and availability. Zinc has been observed to be strongly associated with Mn/Fe (oxyhydr)oxides and phyllosilicates in, for example, the fine-grained fraction of dredged sediment which controlled its behavior in the environment [17]. Consequently, a number of studies have focused on Zn speciation and sorption complexes on discrete Mn oxides [6,8–10] and to a lesser extent in heterogeneous systems representative of soils and sediments [18–20]. X-ray absorption spectroscopic (XAS) techniques have been employed extensively to elucidate sorption mechanisms and obtain molecular-level information. Trivedi and co-workers [6,10] observed outer-sphere complexation of Zn on HMO with octahedral coordination, while Manceau et al. [21] used polarized extended X-ray absorption fine structure spectroscopy (EXAFS) and found substitution of Zn in the interlayer of crystalline birnessite, resulting in a tridentate corner-sharing interlayer complex. Pan et al. [22] reported inner-sphere complexation with edge-sharing linkages between $ZnO_{4,6}$ polyhedron and MnO_6 octahedra in manganite (γ-MnOOH). Bochatay and Persson [8] observed the transformation of a mixture of tetra-

* Corresponding author. Fax: +1 973 596 5790.
E-mail addresses: txb7685@njit.edu (T. Boonfueng), axe@adm.njit.edu (L. Axe), yx3@njit.edu (Y. Xu), tyson@adm.njit.edu (T.A. Tyson).

0021-9797/$ – see front matter
doi:10.1016/j.jcis.2006.01.026

hedral and octahedral complexes on γ-MnOOH to a tetrahedral structure exclusively as pH increased. Zn sorption on Mn oxides has been reported as both outer-sphere to inner-sphere, forming either tetrahedral or octahedral complexes. On other surfaces such as montmorillonite, Lee et al. [23] initially observed a polynuclear complex that transformed to a Zn–Si precipitate as a function of aging. Although its sorption to discrete mineral surfaces has been studied extensively, little has been conducted on Zn complexation with binary substrates of HMO and montmorillonite.

In this study, macroscopic, spectroscopic, and kinetic experiments were employed to investigate the sorption behavior of Zn and the effect of montmorillonite as a substrate for the Mn oxide coating. Adsorption edges and isotherms were conducted to investigate the effect of pH, ionic strength, and surface loading. Concurrently, XAS studies were performed to evaluate the effect of these conditions along with contact time. Moreover, to better understand the slow sorption process, constant boundary condition (CBC) experiments were employed for HMO, HMO-coated clay, and montmorillonite at pH 7 to simulate the subsurface environment. Results from these studies provide a better understanding of zinc speciation and attenuation in the presence of Mn oxide and montmorillonite.

2. Material and methods

2.1. Synthesis and characterization Mn oxide coating

Discrete HMO was prepared according to Gadde and Laitinen [2], while the HMO-coated clay was prepared in the presence of montmorillonite. Na-montmorillonite (Swy-2) was obtained from the Clay Mineral Society [24] and was pretreated to remove of organic matter and other impurities [25]. The specific surface area of montmorillonite from BET analysis was 28 $m^2\,g^{-1}$, which is consistent with others [23]. From potentiometric titrations, the pH point of net zero charge (pH_{pnzc}) was $\sim 4.2 \pm 0.5$ and typically ranges between 2 and 10 [26,27]. Prior to precipitation of HMO on the montmorillonite surface, a suspension of 0.69 $g\,L^{-1}$ montmorillonite in 6.9×10^{-3} M $Mn(NO_3)_2$ was prepared in carbonate free deionized (DI) water (by purging with high purity nitrogen gas (1 $L\,min^{-1}$ at 20 psi) and then mixed for 24 h. Sodium permanganate (4.6×10^{-3} M) and NaOH (9.2×10^{-3} M) were then added and the system was aged for 3 h before centrifuging, rinsing with DI water, and redispersing in 1.5×10^{-2} M ionic strength ($NaNO_3$) for 16 h prior to characterization. The HMO-coated montmorillonite was characterized earlier [16]. Briefly, the coating was observed to be amorphous with uniform coverage on planar surfaces; therefore, HMO dominated the surface charge with the pH_{pnzc} of HMO-coated clay 2.8 ± 0.5. The surface area of the coated systems (95 $m^2\,g^{-1}$) increased while the pore size distribution decreased as compared to the external surface area of montmorillonite and pore size of HMO, respectively. Moreover, XAS of the Mn K-edge revealed that HMO and HMO-coated clay potentially belong to a layered type structure of the phyllomanganate family [16]. However, the long-range structure of the oxide coating was not discernible.

2.2. Adsorption studies

Short-term adsorption studies were conducted with a contact time of 4 h. In these studies, the amount of adsorbate added is fixed, and equilibrium is achieved rapidly with the external surface of the oxide [28]. Adsorption edges and isotherms were used to assess the amount of Zn sorbed to HMO, montmorillonite, and HMO-coated clay as a function pH (1.0–6.0), ionic strength (1.5×10^{-2}–1.5×10^{-1} M $NaNO_3$), and loading which ranged from 10^{-8}–10^{-2} $mol_{Zn}\,g^{-1}_{sorbent}$. Initial concentrations were below the solubility limit of smithsonite, $ZnCO_{3(s)}$ based on Mineql+. All adsorption experiments were conducted in 250-mL polypropylene (Nalgene®) containers under turbulent hydraulic conditions. One $g\,L^{-1}$ and 10^{-1} $g\,L^{-1}$ of oxides and coatings, respectively, were prepared for pH-edge and isotherm studies. Solutions of 10^{-2} and 10^{-1} N of NaOH and HNO_3 were used for adjusting the pH, and stock solutions of Zn nitrate were tagged with the radioactive isotope ^{65}Zn. After 4 h, samples were collected and filtered using a 0.2 μm glass membrane. The percent Zn sorbed on filter and container was negligible. Zinc analyses were performed by measuring the activities of ^{65}Zn in the total suspension and in the filtrate with a Beckman LS6500 Multipurpose scintillation counter. Long-term adsorption studies were required for evaluating the slow sorption process of intraparticle diffusion along microporous surfaces (see, e.g., [6,28]). To observe this process and evaluate experimental diffusivities in a convenient time frame, CBC studies were conducted with HMO, HMO-coated clay, and montmorillonite. The zinc ion concentration in the bulk aqueous phase was maintained constant by monitoring and adding stock solution as needed.

2.3. X-ray absorption spectroscopy (XAS)

Spectra were acquired on beamline X11A of the National Synchrotron Light Source at Brookhaven National Laboratory, where the electron beam energy was 2.8 GeV with a beam current of 260–280 mA. All spectra were collected at the Zn K-edge (9.659 keV) using a Si (111) crystal monochromator over the energy range of 9.509 to 10.408 keV. The wet pastes of Zn sorbed on HMO, HMO-coated clay, and montmorillonite were loaded into acrylic sample holders and sealed with Kapton windows to prevent the loss of moisture. Data were collected from transmission and fluorescence modes with nitrogen gas in the ion chamber before (I_0) and after (I_t) the sample. Samples were placed at 45° to the incident beam using a Lytle detector filled with argon gas to collect fluorescence spectra. Harmonic rejection was achieved by detuning 30% of I_0.

The XAS spectra were analyzed using WinXAS (Version 2.3) [29] following standard procedures [30]. Background X-ray absorbance was subtracted by fitting a linear polynomial through the pre-edge region, and the edge jump of a background-corrected spectrum was normalized with a zero order polynomial over 9.759–9.859 keV. The threshold energy (E_0) was determined from the first inflection point in the edge region and was used to convert the spectra from energy to k-space. An advanced spline function was employed to subtract

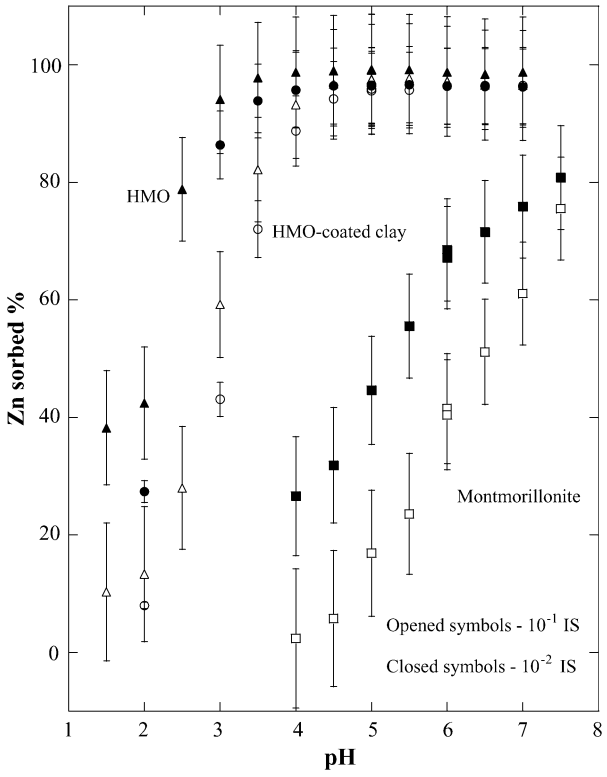

Fig. 1. Zn adsorption edges of HMO, HMO-coated clay, and montmorillonite with 10^{-1} $g_{sorbent}\,L^{-1}$, 10^{-9} M $[Zn]_0$, a $NaNO_3$ based electrolyte, and 25 °C.

the isolated atomic absorption over the range 1.85–13.97 $Å^{-1}$ and convert the X-ray absorption fine structure (XAFS) spectra to ($\chi(k)$), which were weighted by k^3 to enhance the higher k-space data. A Bessel window function was used in Fourier transforms to produce the radial structure function (RSF) over 2.21–10.00 $Å^{-1}$ for all standards and samples. RSFs were fit with the reference model chalcophanite, $ZnMn_3O_7{\cdot}3H_2O$ [31], generated using FEFF7 [32]. The ratio of fluorescence to transmission spectra for 10^{-2} M $Zn(NO_3)_{2(aq)}$ revealed an average S_0^2 of 0.80; this approach has been demonstrated effective [33]. Samples from adsorption studies were used where the sorbed Zn concentrations were measured based on the activity of ^{65}Zn in duplicate studies. Suspensions were centrifuged at 10,000 rpm for 20 min to obtain the wet paste. Samples included ones from CBC studies with aging up to 4 months as well as short-term samples addressing the effect of sorbent (HMO, HMO-coated clay and montmorillonite), adsorbate loading from 10^{-4} to 10^{-2} $mol_{Zn}\,g^{-1}_{sorbent}$, pH 5–7, and ionic strength from 10^{-3} to 10^{-2} ($NaNO_3$ based). Given the volume of the wet paste (∼1 mL) after centrifugation (and even if the entire volume consisted of water) the Zn concentration remaining in the aqueous phase would be 5×10^{-6} M for the greatest loading, two to four orders of magnitude less than the sorbed concentration and therefore not impacting the spectra. In fitting, all parameters were floated and the edge energy was constrained to being equivalent for all shells in the fit. First, each shell was isolated and fit, and was proceeded by multiple shell fitting over a radial window of 0.50–3.70 Å.

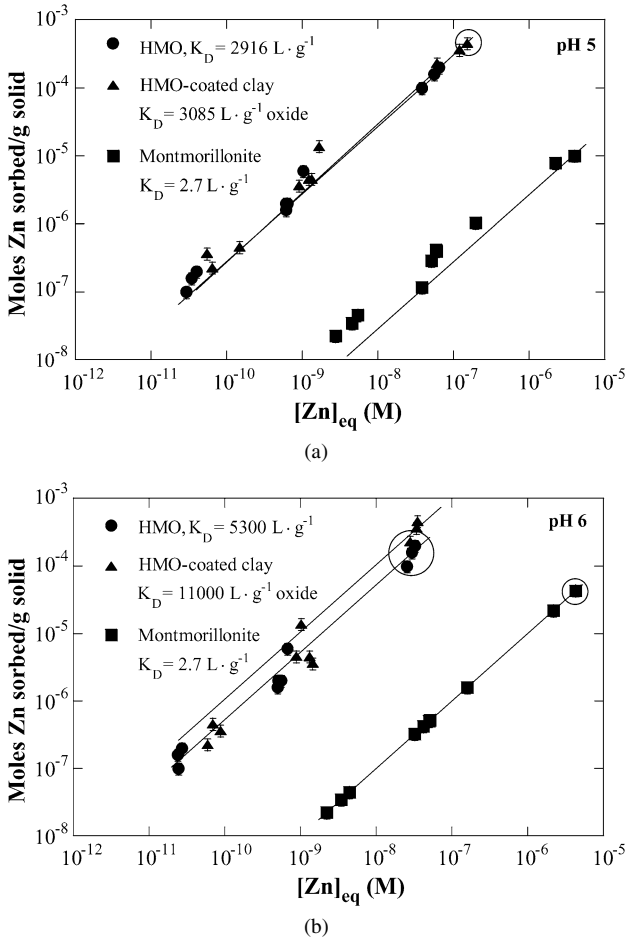

Fig. 2. Zn adsorption isotherms for HMO, HMO-coated clay, and montmorillonite at pH 5 and 6, 1.5×10^{-2} ionic strength ($NaNO_3$), and 25 °C. Adsorption to HMO-coated clay has been normalized to HMO present, showing the linear relationship ($mol_{Zn\ sorbed}\,g^{-1}_{sorbent} = K_D\,[Zn]_{eq}$, where R^2 is greater than 0.8 and the error of K_D is approximately 30%). Circles identify XAS samples.

3. Results and discussion

3.1. Macroscopic adsorption study

Adsorption edges (Fig. 1) reveal the effect of ionic strength was clearly observed for adsorption to montmorillonite, suggesting outer-sphere complexes. Strawn et al. [34] observed this type of complex when Pb sorbed to permanently charged ion exchange sites of montmorillonite [34]. For HMO, ionic strength effects were only seen at a pH less than 4 and for a pH greater than 4, sorption may be dominated by inner-sphere complexes. Li et al. [9] too observed similar edges at pH greater than 4. In isotherms at pH 5 and 6 (Fig. 2), the linear relationship between the sorbed and bulk aqueous concentrations suggests that adsorption can be described with one average type of site. Given the limited solubility of Zn, the isotherm was not observed to plateau, indicating a significant site capacity as reported by others [35–37], ranging from 10^{-3} to 10^{-2} $mol_{metal\ ion}\,g^{-1}$. Interestingly, normalizing the sorbed Zn on HMO-coated clay to the amount of oxide present as coating (∼0.32 $g_{Mn}\,g^{-1}_{clay}$ [16]) reveals similar sorption affinity to that of HMO. Nevertheless, the distribution coefficient

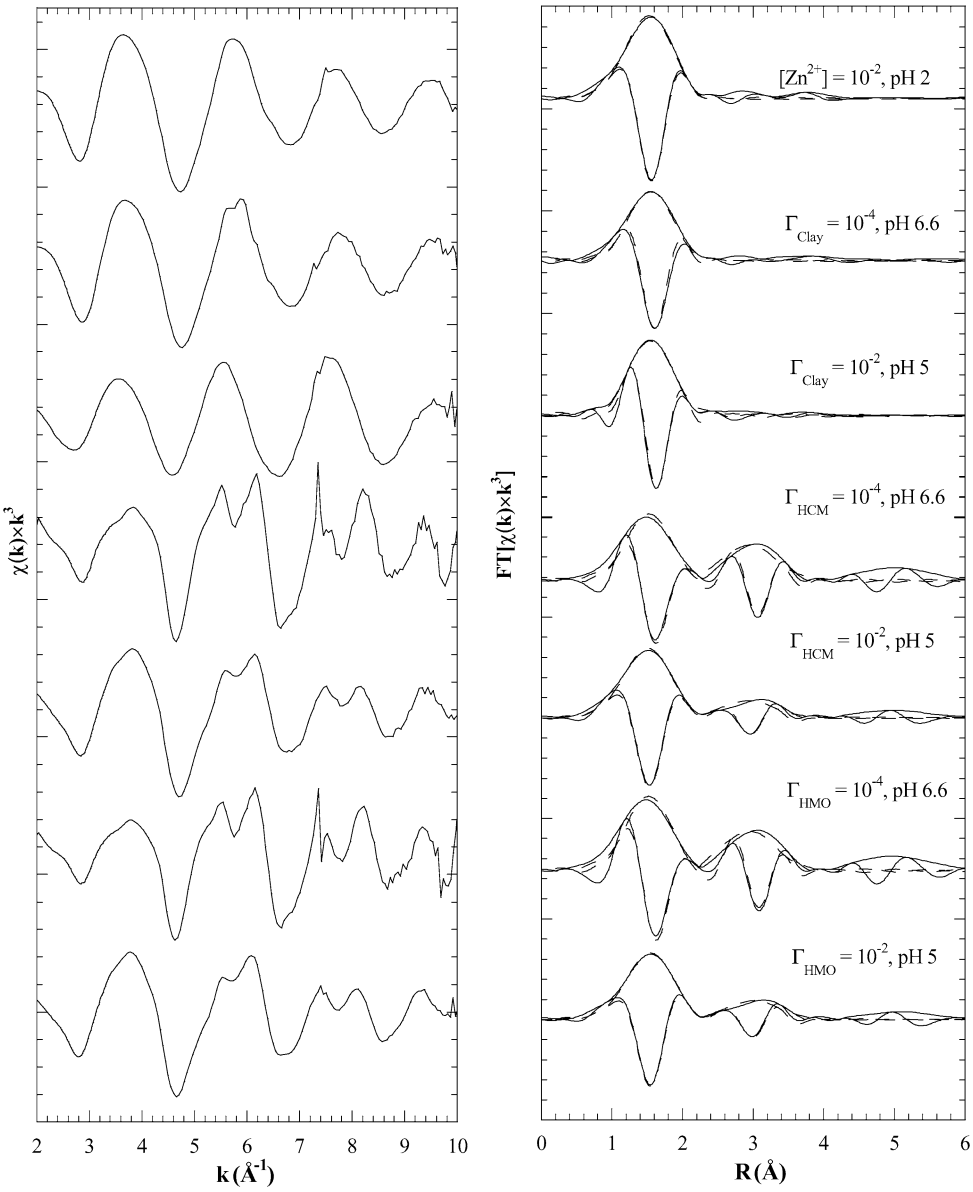

Fig. 3. Zn K-edge $\chi(k) \cdot k^3$ spectra of Zn standard and Zn sorption samples as a function of surface loading ($\Gamma_{\text{solid}} = \text{mol}_{\text{Zn}}\, \text{g}^{-1}_{\text{solid}}$) with 10^{-2} ionic strength ($NaNO_3$) (collected at 25 °C along with Fourier transformed $\chi(k) \cdot k^3$ spectra over 2.21–10.00 $Å^{-1}$ and fitted over 0.50–3.70 Å. Solid lines represent the data and dashed lines are the fit. HCM represents HMO-coated clay.

(K_D) of coated systems increases as compared to discrete systems, suggesting that morphological changes may result in increased site capacity. These short-term studies suggest that Mn oxide is a dominant surface for sorption. In following section, the sorption configuration of Zn was investigated by using XAS.

3.2. XAS analysis of Zn sorption

XAS spectra of Zn sorbed onto montmorillonite were relatively similar to aqueous Zn^{2+} (Fig. 3). The fitting revealed 4.0–6.0 atoms of oxygen at a distance of 2.06 ± 0.02 Å in the first shell (Table 1A), suggesting that upon adsorption Zn does not lose its waters of hydration. Moreover, a second shell was not observed, again consistent with outer-sphere complexation. In contrast to this work, Lee et al. [23] observed that initially Zn formed surface precipitates on montmorillonite at pH 7, which transformed to a Zn-phyllosilicate-like phase after 20 days. Similar results were reported by Trainor et al. [38], where Zn formed a mixed-metal Zn(II)–Al(III) coprecipitate with a hydrocalcite-type structure between pH 7 and 8.2. In this study, surface precipitation was not observed for pH less than 7.

Comparing spectra for Zn sorbed on HMO-coated clay to HMO, similar envelopes are seen (Fig. 3). The first shell was fitted well with oxygen and second shell contributions were attempted with Si, Al, Zn, and O as well as combinations of these, but fitting was only accomplished with Mn. The amplitude of the second shell in lower surface loadings (10^{-4} $\text{mol}_{\text{Zn}}\, \text{g}^{-1}_{\text{sorbent}}$) was greater than that of higher loadings (10^{-2} $\text{mol}_{\text{Zn}}\, \text{g}^{-1}_{\text{sorbent}}$)

Table 1
Fitting results for the first (O) and second (Mn) shells. Zn K-edge $\chi(k) \cdot k^3$ spectra were Fourier transformed over 2.21–10.00 Å^{-1} in k-space and fitted over 0.50–3.70 Å in r-space

	O			Mn			ΔE_0 (eV)	%Res
	N_1	R (Å)	σ^2 (Å^2)	N_2	R (Å)	σ^2 (Å^2)		
(A) Zn sorption as a function of sorbent and surface loading with 4 h reaction time								
$Zn(NO_3)_{2(aq)}$	5.7	2.06	0.0136	–	–	–	−1.64	7.3
$\Gamma_{Clay} = 10^{-4}$, pH 6.6, IS 10^{-2}	6.0	2.05	0.0053	–	–	–	−1.12	11.5
$\Gamma_{Clay} = 10^{-2}$, pH 5, IS 10^{-2}	4.0	2.06	0.0008	–	–	–	−7.60	9.6
$\Gamma_{HMO} = 10^{-4}$, pH 6.6, IS 10^{-2}	6.9	2.05	0.0091	4.6	3.45	0.0069	−4.10	16.6
$\Gamma_{HMO} = 10^{-2}$, pH 5, IS 10^{-2}	6.6	2.06	0.0135	2.5	3.50	0.0099	0.57	8.8
$\Gamma_{HCM} = 10^{-4}$, pH 6.6, IS 10^{-2}	6.6	2.05	0.0093	3.9	3.45	0.0058	−3.48	16.6
$\Gamma_{HCM} = 10^{-2}$, pH 5, IS 10^{-2}	7.7	2.04	0.0147	2.4	3.45	0.0109	−1.83	10.9
(B) Zn sorbed on HMO-coated clay as a function of pH, surface loading, and ionic strength with 4 h reaction time								
$\Gamma_{HCM} = 10^{-2}$, pH 6, IS 10^{-2}	7.6	2.01	0.0150	1.2	3.40	0.0079	−3.22	12.8
$\Gamma_{HCM} = 10^{-3}$, pH 5, IS 10^{-2}	6.8	2.08	0.0130	3.2	3.50	0.0111	0.17	8.8
$\Gamma_{HCM} = 10^{-2}$, pH 5, IS 10^{-1}	7.7	2.06	0.0152	2.6	3.48	0.0110	−1.19	10.9
(C) Zn sorbed on HMO-coated clay as a function of contact time								
$\Gamma_{HCM} = 10^{-3}$, pH 7, IS 10^{-2}	7.5	2.01	0.0152	1.4	3.45	0.0025	−6.24	9.5
$\Gamma_{HCM} = 10^{-3}$, pH 7, IS 10^{-2} (CBC 1 month)	5.5	2.03	0.0098	4.1	3.43	0.0134	−0.71	11.2
$\Gamma_{HCM} = 1.5 \times 10^{-3}$, pH 7, IS 10^{-2} (CBC 4 month)	5.0	2.04	0.0095	4.5	3.43	0.0151	0.81	10.0

Γ is surface loading ($\Gamma_{solid} = mol_{Zn}\, g^{-1}_{solid}$). N, R, and σ^2 represent the coordination number, distance, and variance. The quality of fits for N_1, N_2, R, and σ^2 are ±20%, ±40%, ±0.02, and ±5%, respectively.

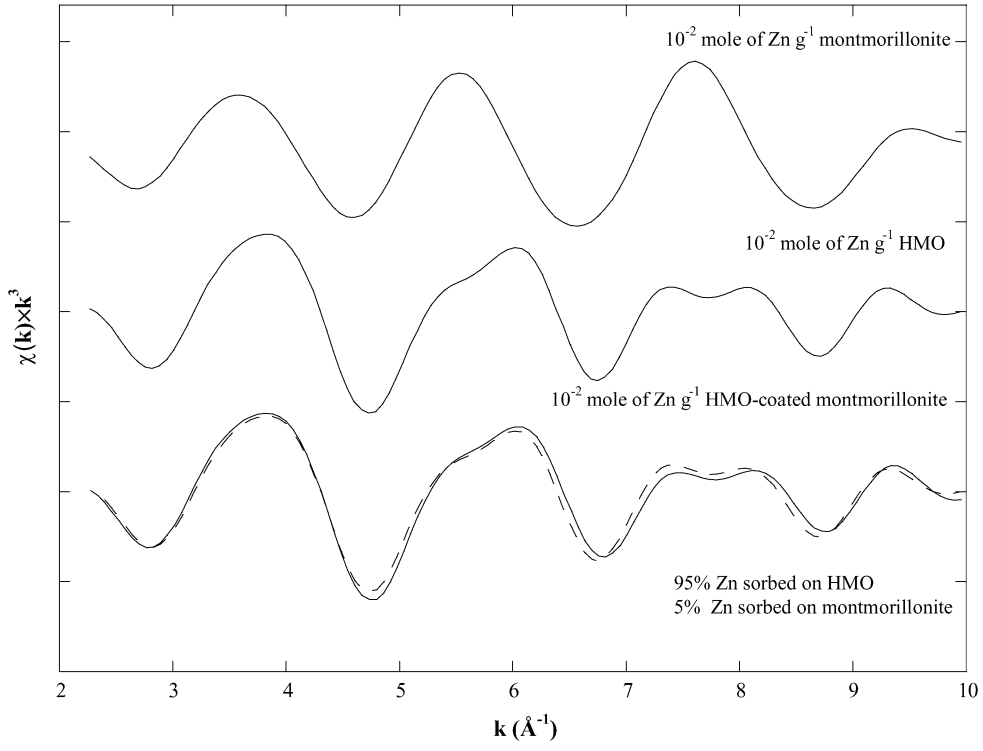

Fig. 4. Inverse Fourier transform of the Zn sorption samples as a function of sorbent ($\Gamma_{solid} = 10^{-2}\ mol_{Zn}\, g^{-1}_{solid}$) at pH 5 and 10^{-2} ionic strength ($NaNO_3$). Solid lines represent the data and dashed line is the LC fit of HMO-coated clay with 95% from Zn sorbed on HMO and 5% from Zn sorbed on montmorillonite.

(Fig. 3) and may be a result of a greater degree of disorder (σ^2) for the latter which would suppress the amplitude of the second shell. Moreover, linear combination (LC) fitting based on principle component analysis involved using back Fourier Transformed data of Zn sorbed to HMO and montmorillonite at the same condition and resulted in a 95% contribution from sorption to HMO and 5% from that of montmorillonite (Fig. 4). The montmorillonite substrate potentially increases the site density of the system; furthermore, it may contribute to morphological changes in the HMO coating compared to the discrete mineral form. XAS spectra of Zn sorbed onto HMO-coated clay at pH 5 revealed that the sorption configuration was invariant as a function of surface loading and ionic strength, 10^{-1} and 10^{-2} ($NaNO_3$) (Fig. 4 and Table 1B). An average of the fitting results

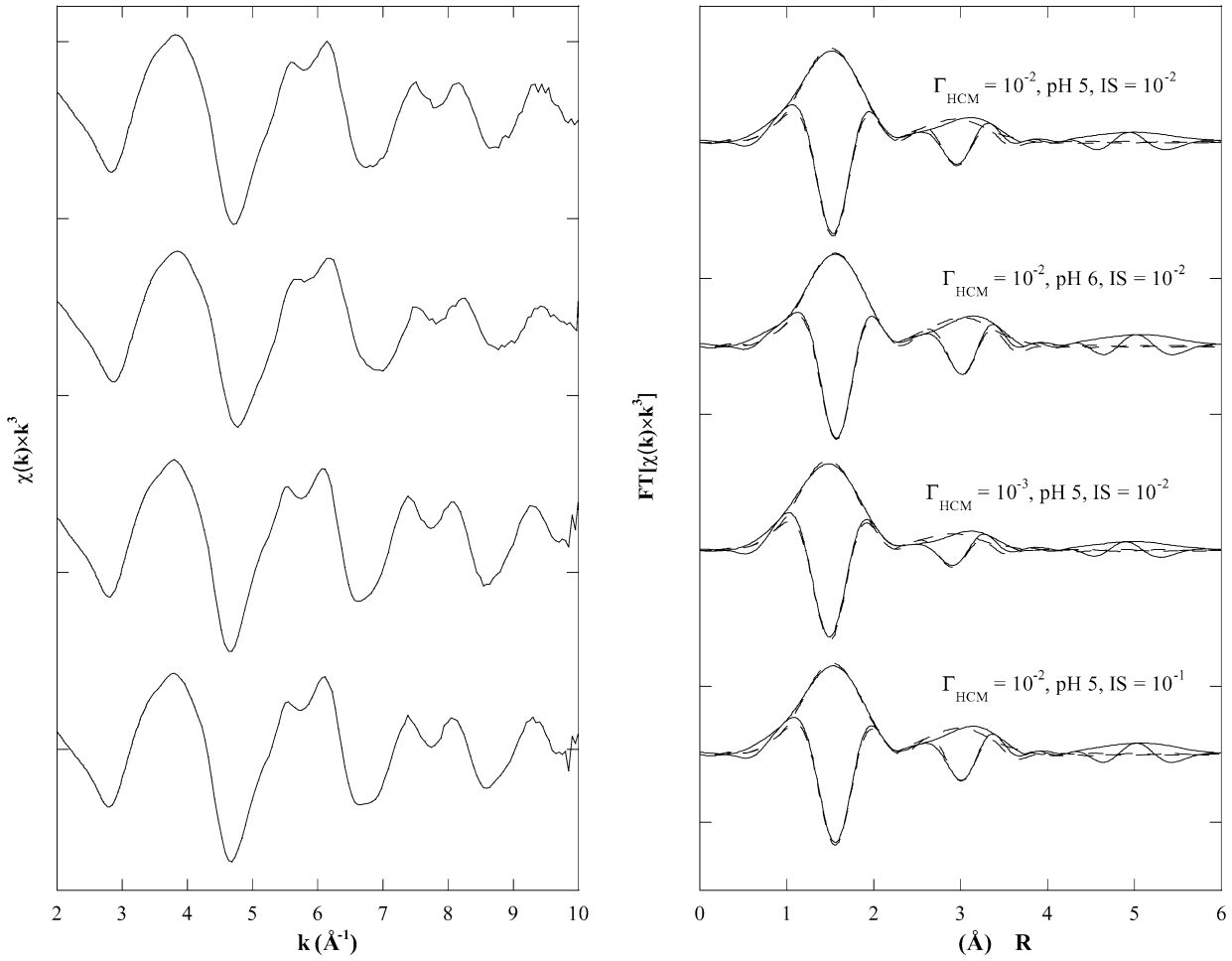

Fig. 5. Zn K-edge $\chi(k)\cdot k^3$ spectra of Zn sorption on HMO-coated clay as a function of pH, surface loading, and ionic strength collected at 25 °C along with Fourier transformed $\chi(k)\cdot k^3$ spectra over 2.21–10.00 Å^{-1} and fitted over 0.50–3.70 Å. Solid lines represent the data and dashed lines are the fit.

showed a first shell of 7.3 ± 0.9 atoms of oxygen at a distance of 2.06 ± 0.02 Å, while in the second shell 3.2 ± 1.2 atoms of manganese were found at 3.47 ± 0.02 Å. Interestingly, these bond distances are relatively similar to Zn sorbed on birnessite [21], suggesting octahedral coordination and tridentate corner sharing complexes when sorbed on HMO and HMO-coated clay. Trivedi et al. [10] observed approximately 7 oxygen atoms in the first shell and 8 atoms of oxygen in the second shell, concluding that the Zn ion retained its primary hydration shell. In our study, while the first shell structure was equivalent to that modeled by Trivedi et al., Fourier transforms were applied over 2.21–10.00 Å^{-1} and Trivedi et al. used 2.4–9.4 Å^{-1}. Because of the increased k-space, second shell contributions have been refined.

For loadings greater than 10^{-4} $\mathrm{mol_{Zn}\,g^{-1}_{sorbent}}$, as pH increased from 5 to 7, the first shell distance decreased potentially due to an increase in electrostatic interactions between Zn ions and the surface (Figs. 5, 6 and Table 1). The effect of loading was not clearly observed in this study; however, Manceau et al. [21] found that Zn sorbed as tridentate complexes on birnessite with tetrahedral coordination at low surface coverage ($\sim 8.0\times10^{-3}$ $\mathrm{mol_{Zn}\,mol_{Mn}}$) and octahedral coordination at high surface coverage ($>6.9\times10^{-2}$ $\mathrm{mol_{Zn}\,mol_{Mn}}$). Nevertheless, our work is consistent with these results where we have seen octahedral coordination as was reported for the higher surface coverage. In addition to evaluating adsorption mechanisms in batch studies, CBC studies were included to evaluate the slow sorption process.

3.3. Intraparticle surface diffusion of Zn

In the alternative CBC studies, slow sorption was observed for all systems (Fig. 7). Because the oxide, oxide-coated clay, and montmorillonite exhibit microporous structures, the sorption process may be described as a slow intraparticle diffusion. Initially the amount of Zn sorbed corresponds to the isotherm results for that sorbed to the external surface. Subsequently, the amount of Zn sorbed to the oxide gradually increased due to intraparticle surface diffusion. In modeling, the assumption that internal sites are no different than external ones has been validated recently in spectroscopic results for metals ions such as Sr sorbed to hydrous iron and manganese oxide [39,40]. In our work, the local coordination of Zn sorbed to HMO-coated clay from a 4-month CBC study (where an additional 60% of the sites became occupied as compared to 4 h contact time) (Fig. 6 and Table 1C) revealed that as surface loadings increased from

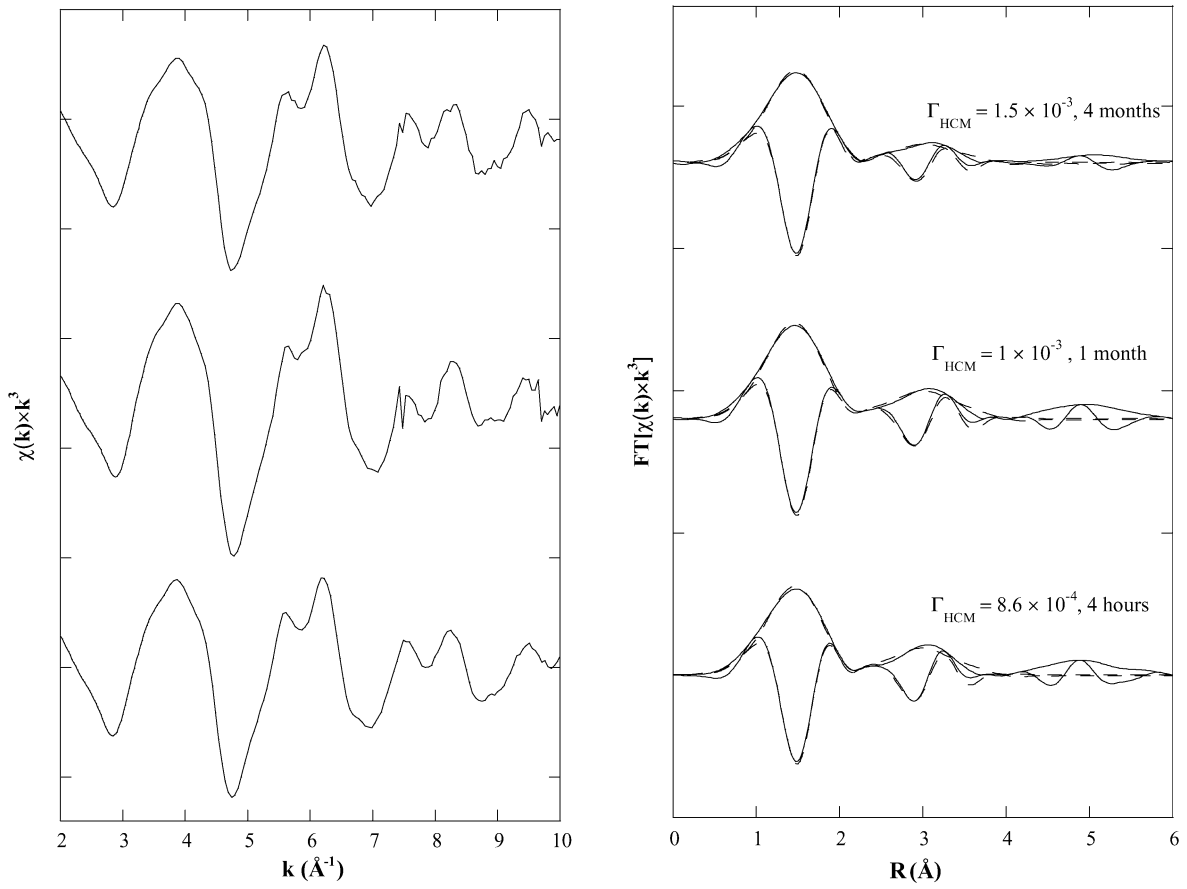

Fig. 6. Zn K-edge $\chi(k) \cdot k^3$ spectra of HMO-coated clay as a function of contact time at pH 7, 1.5×10^{-2} ionic strength ($NaNO_3$) were collected at 25 °C and Fourier transformed over 2.21–10.00 $Å^{-1}$ and fitted over 0.50–3.70 Å.

8.66×10^{-4} to 1.48×10^{-3} $mol_{Zn}\, g^{-1}_{HMO\text{-}coated\ clay}$, the bond distances of Zn–O and Zn–Mn averaged 2.03 and 3.43 Å, which is consistent with tridentate corner sharing octahedra [21]. Specifically, the Zn structure consisted of 7.3 ± 1.5 atoms of oxygen in the first shell and 4.0 ± 0.6 atoms of manganese in the second. Furthermore, there was no evidence of surface precipitation or solid solution formation as only Mn provided a good fit in the second shell.

In modeling the slow sorption process of intraparticle surface diffusion along micropores, the analytical solution to the mass balance (see, e.g., [41,42]) given the CBC (as well as the initial condition that contaminant was not present initially ($t = 0$)) was integrated over the volume of the particle. Minimizing the variance between experimental data and modeling results, the only fitting parameter is surface diffusivity. Errors associated with the model from the propagation of errors (POE) method [43] are also shown. The POE analysis accounts for the standard deviation in the number of particles as well as the error in the distribution coefficient describing the mass adsorbed to the surface. All data for the HMO systems fall within two standard deviations of the model. However, from the CBC study of Zn sorption to montmorillonite (Fig. 7), a potential change was observed after 25 days contact time. The shift in the amount sorbed may reflect analytical and modeling errors or may be indicative of a change in the sorption mechanism, as Lee et al. [23] observed neoformation of a Zn phyllosilicate phase at the montmorillonite surface after aging 20 days.

Studies with Zn sorption to HMO, HMO-coated montmorillonite, and montmorillonite demonstrate that surface diffusivities (D_S) range from 10^{-18} to 10^{-17} $cm^2\, s^{-1}$. The D_S of HMO-coated clay was 7×10^{-18} $cm^2\, s^{-1}$, which falls between that for montmorillonite and HMO. These results indicate that the microporosity of HMO-coated clay has contributions from both the HMO and montmorillonite surfaces. Furthermore, even though much of the clay surface is coated with HMO (∼90%) based on earlier characterization studies [16]; the oxide morphology is potentially different from discrete ones. We speculate that clay particles serve as a template for Mn oxide when nucleation occurred; potentially changing the porosity, pore size distribution, and particle size of oxide coating. Therefore, the oxide-coated clay may exhibit unique characteristics from the discrete oxide.

4. Conclusion

Macroscopic studies showed that the affinity and capacity of the HMO coating was greater than that of montmorillonite, and when normalized to the oxide present, the coatings behaved similarly to the discrete oxide. A linear relationship was observed for the isotherms at pH 5 and 6. Moreover, XAS resulted in one type of sorption configuration as a function of loading

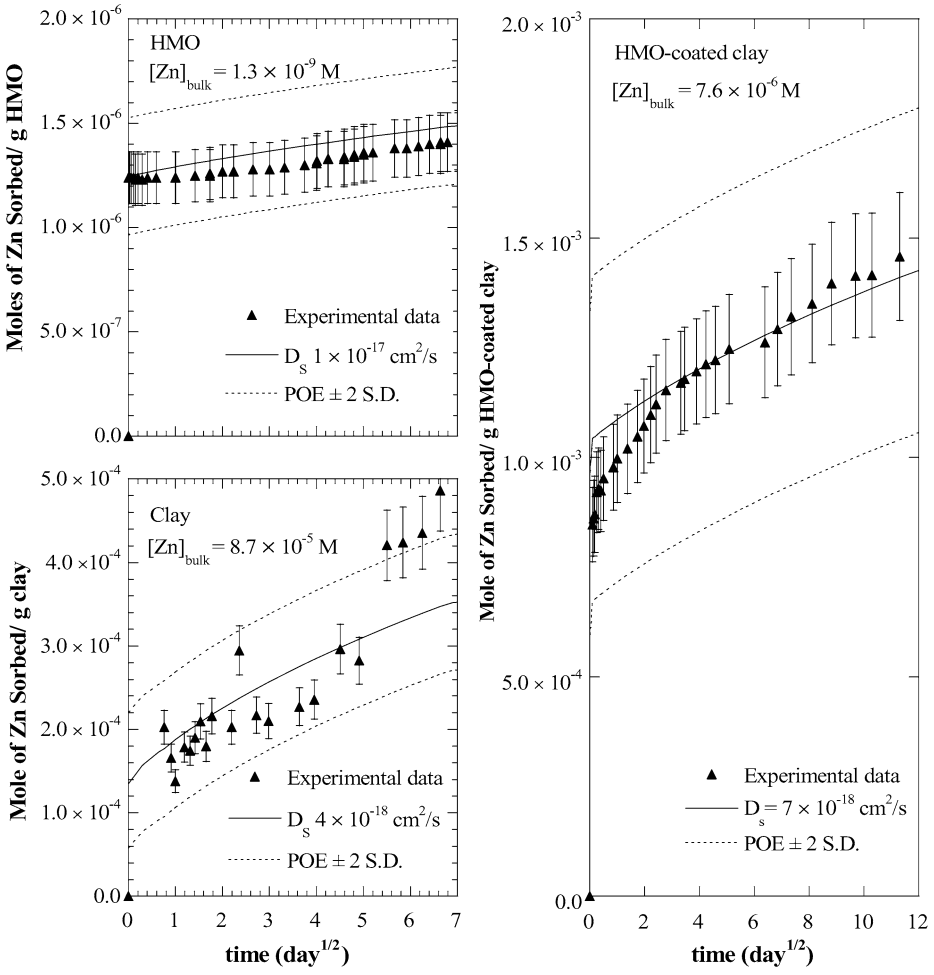

Fig. 7. CBC studies of Zn sorption to 10^{-1} g L^{-1} HMO, HMO-coated clay, and clay at 25 °C, 1.5×10^{-2} ionic strength with $NaNO_3$, pH 7, and a $[Zn]_{bulk}$ of 7.6×10^{-6} M for HMO-coated clay, 1.3×10^{-9} M for HMO, and 8.7×10^{-5} M for clay.

and ionic strength at pH 5. Zn ions appear to associate with the Mn oxide phase where inner-sphere complexes dominate the sorption process, forming tridentate corner-sharing structures. After a contact time of 4 months where an additional 60% of the sites become occupied, the slower sorption process was modeled as intraparticle surface diffusion. Best fit diffusivities ranged from 10^{-18} to 10^{-17} $cm^2\,s^{-1}$, where a slower process was observed for the coated surface as compared to the discrete oxide. Interestingly, the porosity of the Mn oxide coating appears to be influenced by the substrate during its growth, as its increase and shift to a smaller pore size distribution resulted in a diffusivity between that observed for discrete HMO and montmorillonite.

Acknowledgments

This material is based upon work supported by the National Science Foundation under Grant No. BES 0089903 and the DuPont Young Professor's Grant. The authors thank James A. Dyer and Noel C. Scrivner for their input and support. The authors also thank Kaumudi Pandya for technical support at beamline X11A. Research carried out at NSLS, Brookhaven National Laboratory, was supported in part by the U.S. Department of Energy, Division of Materials Sciences and Division of Chemical Sciences, under Contract No. DE-AC02-98CH10886. In addition, beamline X11 at NSLS is supported by the Office of Naval Research. Finally, the authors thank an anonymous reviewer for the helpful comments.

References

[1] S.A. Carroll, P.A. O'Day, M. Piechowski, Environ. Sci. Technol. 32 (1998) 956–965.
[2] R.R. Gadde, H. Laitinen, Anal. Chem. 46 (1974) 2022–2026.
[3] H. Green-Pederson, B.T. Jensen, N. Pind, Environ. Technol. 18 (1997) 807–815.
[4] L.W. Lion, R.S. Altmann, J.O. Leckie, Environ. Sci. Technol. 16 (1982) 660–666.
[5] Y.W. Nelson, L.W. Lion, M.L. Shuler, W.C. Ghiorse, Environ. Sci. Technol. 36 (2002) 421–425.
[6] P. Trivedi, L. Axe, Environ. Sci. Technol. 34 (2000) 2215–2223.
[7] L. Axe, T. Tyson, P. Trivedi, T. Morrison, J. Colloid Interface Sci. 224 (2000) 408–416.
[8] L. Bochatay, P. Persson, J. Colloid Interface Sci. 229 (2000) 593–599.
[9] X. Li, G. Pan, Y. Qin, T. Hu, Z. Wu, Y. Xie, J. Colloid Interface Sci. 271 (2004) 35–40.
[10] P. Trivedi, L. Axe, T. Tyson, Environ. Sci. Technol. 35 (2001) 4515–4521.
[11] R.M. Potter, G.R. Rossman, Am. Mineral. 64 (1979) 1219–1226.
[12] L.S. Balistrieri, J.W. Murray, Geochim. Cosmochim. Acta 46 (1982) 1041–1052.

[13] D. Dong, Y.M. Nelson, L.W. Lion, L. Shuler, W.C. Ghiorse, Water Res. 34 (2000) 427–436.
[14] A. Manceau, N. Tamura, R.S. Celestre, A.A. Macdowell, N. Geoffroy, G. Sposito, H.A. Padmore, Environ. Sci. Technol. 37 (2003) 75–80.
[15] K.W. Manderneck, J. Post, B.M. Tebo, Geochim. Cosmochim. Acta 59 (1995) 4393–4408.
[16] T. Boonfueng, L. Axe, Y. Xu, J. Colloid Interface Sci. 281 (2005) 80–92.
[17] M.P. Isaure, A. Laboudigue, A. Manceau, G. Sarret, C. Tiffreau, P. Trocellier, G. Lamble, J.L. Hazemann, D. Chateigner, Geochim. Cosmochim. Acta 66 (2002) 1549–1567.
[18] D.R. Roberts, A.C. Scheinost, D.L. Sparks, Environ. Sci. Technol. 36 (2002) 1742–1750.
[19] G.D. Robinson, Chem. Geol. 33 (1981) 65–79.
[20] A.C. Scheinost, R. Kretzschmar, S. Pfister, D.R. Roberts, Environ. Sci. Technol. 36 (2002) 5021–5028.
[21] A. Manceau, B. Lanson, V.A. Drits, Geochim. Cosmochim. Acta 66 (2002) 2639–2663.
[22] G. Pan, Y. Qin, X. Li, T. Hu, Z. Wu, Y. Xie, J. Colloid Interface Sci. 271 (2004) 28–34.
[23] S. Lee, P.R. Anderson, G.B. Bunker, C. Karafil, Environ. Sci. Technol. 38 (2004) 5426–5432.
[24] P.A. Costanzo, S. Guggenheim, Clays Clay Miner. 49 (2001) 433–443.
[25] G.W. Kunze, J.B. Dixon, in: A. Kulte (Ed.), Method of Soil Analysis: Physical and Mineralogical Methods, American Society of Agronomy/Soil Science Society of America, Madison, WI, 1982, p. 91.
[26] L. Mitchill, Ceramics-Stone Age and Space Age, McGraw–Hill, New York, 1963.
[27] W. Stumm, Chemistry of the Solid–Water, Interface, Wiley, New York, 1992.
[28] L. Axe, P. Anderson, J. Colloid Interface Sci. 185 (1997) 436–448.
[29] T. Ressler, J. Synchrotron Radiation 5 (1998) 118–122.
[30] B. Bunker, D. Sayers, in: D.C. Koningsberger, R. Prins (Eds.), X-Ray Absorption: Principles, Applications, Techniques of EXAFS, SEXAFS, and XAFS, Wiley, New York, 1988.
[31] J.E. Post, D.E. Appleman, Am. Mineral. 73 (1988) 1401–1404.
[32] S.I. Zabinsky, J.J. Rehr, A. Aukudinov, R.C. Albers, M.J. Eller, Phys. Rev. B 52 (1995) 2995–3009.
[33] L. Tröger, D. Arvanitis, K. Baberschke, H. Michaelis, U. Grimm, E. Zschech, Phys. Rev. B 46 (1992) 3283–3289.
[34] D.G. Strawn, D.L. Sparks, J. Colloid Interface Sci. 216 (1999) 257–269.
[35] P. Trivedi, L. Axe, J. Colloid Interface Sci. 218 (1999) 554–563.
[36] H. Tamura, N. Katayoma, R. Furuichi, J. Colloid Interface Sci. 195 (1997) 192–202.
[37] C. Kennedy, S.D. Smith, L.A. Warren, Geochim. Cosmochim. Acta 68 (2004) 443–454.
[38] T.P. Trainor, G.A. Gordon, B.E. Parks, J. Colloid Interface Sci. 231 (2000) 359–372.
[39] L. Axe, P. Trivedi, T. Morrison, J. Colloid Interface Sci. 224 (2000) 408–416.
[40] L. Axe, G.B. Bunker, P.R. Anderson, T. Tyson, J. Colloid Interface Sci. 199 (1998) 44–52.
[41] L. Axe, P. Trivedi, J. Colloid Interface Sci. 247 (2002) 259–265.
[42] L. Axe, P.R. Anderson, J. Colloid Interface Sci. 175 (1995) 157–165.
[43] H.H. Ku, J. Res. Natl. Bur. Standards C: Eng. Instrum. 70 (1966) 263–273.